Slow light for deep tissue imaging with ultrasound modulation

Huiliang Zhang,[1,a)] Mahmood Sabooni,[2] Lars Rippe,[2] Chulhong Kim,[3,b)] Stefan Kröll,[2] Lihong V. Wang,[3] and Philip R. Hemmer[1,c)]
[1]*Department of Electrical and Computer Engineering, Texas A&M University, College Station, Texas 77843, USA*
[2]*Department of Physics, Lund University, Box 118, S-221 00 Lund, Sweden*
[3]*Department of Biomedical Engineering, Washington University in St. Louis, St. Louis, Missouri 63130, USA*

(Received 6 February 2012; accepted 5 March 2012; published online 26 March 2012)

Slow light has been extensively studied for applications ranging from optical delay lines to single photon quantum storage. Here, we show that the time delay of slow-light significantly improves the performance of the narrowband spectral filters needed to optically detect ultrasound from deep inside highly scattering tissue. We demonstrate this capability with a 9 cm thick tissue phantom, having $10\,\mathrm{cm}^{-1}$ reduced scattering coefficient, and achieve an unprecedented background-free signal. Based on the data, we project real time imaging at video rates in even thicker phantoms and possibly deep enough into real tissue for clinical applications like early cancer detection. © *2012 American Institute of Physics*. [http://dx.doi.org/10.1063/1.3696307]

Optical imaging deep inside highly scattering materials can be accomplished using ultrasound to selectively modify or "tag" the light that is scattered by the object of interest, for example a tumor surrounded by healthy tissue.[1] This approach maintains the advantages of optical imaging, like sensitivity to color and texture which provides information on chemical content and biological function, but the resolution is determined by the ultrasound which is far less degraded by the scatter in the surrounding material.[2] Yet, to see small objects buried deep inside a scattering medium, an efficient filtering technique is required to remove the substantial noise due to background scattered light. In the case of ultrasound modulation, this can be accomplished by selectively filtering out light at the ultrasound modulated frequencies. However due to the highly diffuse nature of the scattered light, most optical filtering techniques do not perform well enough to allow small objects buried deep inside larger ones to be detected. This has so far prevented ultrasound modulated optical tomography from finding clinical applications. Here, we show that using slow light[3] in addition to a high performance spectral hole burning type filter[4] can finally reach this elusive goal. In particular, we show that ultrasound modulated light coming from deep inside an unprecedented 9 cm thick tissue phantom can be seen without detectable background. From this data and measurements made in real tissue, we show that straightforward improvements in the experimental setup would allow video rate imaging in even thicker tissue such as the breast or brain. This unique application of slow light and ultrasound opens the door to eventual clinical applications of ultrasound modulated optical tomography as well as numerous commercial and military applications like optical imaging through clouds, underwater, and in harsh manufacturing environments.

Optical imaging is normally the preferred technique for examining biological tissues and many other objects of interest in commercial, military, and scientific applications. In addition to the selectivity to color and texture, it has the potential for remote detection, and non-invasive imaging. Ultrasound imaging can give high resolution where optical imaging cannot, such as for highly scattering objects when a high depth to resolution ratio is required, but ultrasound images are mainly limited to mechanical contrast,[5] which do not give nearly as much chemical or biological information, and are subject to speckle artifacts.

To overcome the limitations of ultrasound imaging, a number of techniques involving optically generated and detected ultrasound have been developed. These techniques seek to keep the advantages of optical imaging even in highly diffuse media while maintaining the resolution of ultrasound imaging. For example, optical detection of ultrasound is routinely used for quality monitoring in harsh manufacturing environments,[6] and it has been demonstrated for remote environmental hazard monitoring.[7] When the optical detection of ultrasound is applied to biological imaging, it is known as ultrasound optical tomography (UOT) or acousto-optic tomography (AOT).[2] Compared to conventional ultrasound imaging, UOT images can have both optical and mechanical contrast in addition to being free of ultrasound speckle artifacts.[8] Likewise, the optical generation of ultrasound has led to powerful applications like photoacoustic spectroscopy for trace chemical detection which has multiple commercial and military uses.[9] When applied to biological imaging, this is known as photoacoustic tomography (PAT) and has shown great promise for imaging inside highly scattering tissue.[10] UOT and PAT can be viewed as complementary technologies because UOT produces images by the optical detection of ultrasound whereas PAT produces images by the optical generation of ultrasound.[1]

The basic physics of optically detected ultrasound is illustrated in Figure 1(a). Briefly, ultrasound produces high and low pressure regions inside the scattering medium which changes the local density of optical scattering centers and also

[a)]Now at Department of Physics, Harvard University, Cambridge, Massachusetts 02138, USA.
[b)]Now at Department of Biomedical Engineering, University at Buffalo, The State University of New York, Buffalo, New York 14260-2050, USA.
[c)]Author to whom correspondence should be addressed. Electronic mail: prhemmer@ece.tamu.edu.

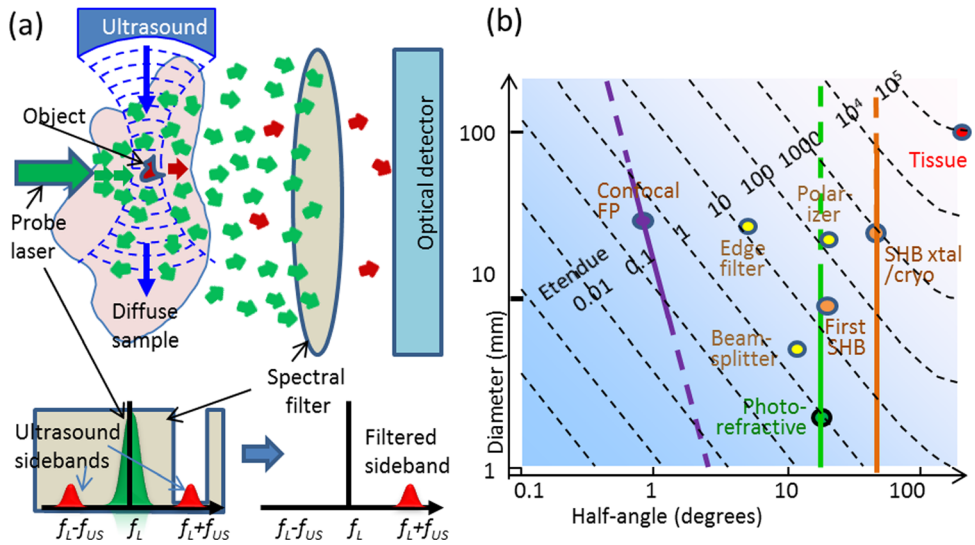

FIG. 1. (a) Optically detected ultrasound imaging inside a highly scattering medium. The probe light is modulated in the ultrasound region, for example at the location of the embedded object. This creates modulation sidebands on the probe light at plus and minus the ultrasound frequency. Since the sideband power depends on the optical and acoustic properties of the object, the image includes both optical and acoustic contrast. The spectral filter passes only one sideband with high discrimination. For demanding applications, a modulated signal of only a few photons will be produced even using Watts of illumination power. (b) Contour plot of units of steradians-mm^2 vs diameter and half angle. Solid lines show reasonable ranges for the three leading techniques, confocal FP, photorefractive, and SHB. Dots show particular cases discussed in text.

the refractive index via the acousto optic effect. This causes amplitude and phase modulation of the probe light at the ultrasound frequency, producing new optical frequencies, or sidebands, shifted from the original by +/- the ultrasound frequency, as illustrated in Figure 1(a). Monitoring the intensity of this ultrasound "tagged" light while scanning the ultrasound focus produces an image of the interior of the object.

The main technical challenge arises when applying ultrasound enhanced optical imaging to highly scattering objects as in deep tissue UOT. Here the ultrasound tagged

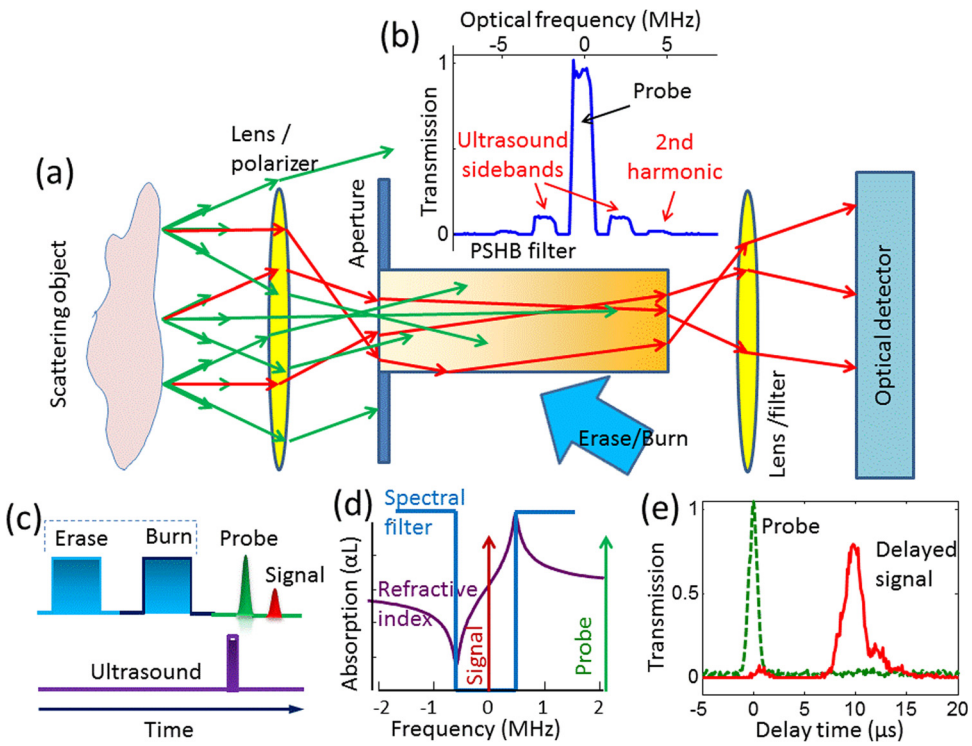

FIG. 2. (a) Schematic of spectral hole and slow light filtering setup. Scattered light from the sample is collected by a lens and passed through a persistent spectral hole burning (PSHB) filter. The filtered sideband (tagged) light is then sent through a fluorescence filter and imaged onto a sensitive photodetector. (b) Convolution of the spectral filter and ultrasound modulation spectrum for a 2.5 cm thick tissue phantom. The spectral filtering hole has a square shape, which was chosen to give the largest dynamic range. (c) Conceptual diagram of the optical and ultrasound pulse sequence. The spectral hole is created by first initializing, or erasing, any previous spectral holes. The desired hole is then engraved using a precise pulse sequence (denoted "Burn"). The ultrasound is applied and optically probed after some propagation delay. (d) A deep spectral hole also has a steep refractive index dispersion at its center, which gives a slow group velocity for the tagged light signal. (e) For a sufficiently short optical probe pulse, slow light gives complete temporal discrimination between the tagged and untagged light.

light is typically many orders of magnitude weaker than the background "untagged" light.[11] This is caused by the low light intensity deep inside tissue[2] and the small focused ultrasound volume used to get high resolution. The key task is then to efficiently extract this weak tagged light from the much stronger background or more precisely from the noise produced by the background. In Figure 1(a), this is illustrated by a spectral filter that absorbs the untagged light while allowing tagged light to pass with minimal attenuation. Another option is heterodyne detection, but this is most applicable to non-scattering objects. To collect as much of the tagged light as possible, the etendue, defined by the product of the light solid angle and area,[12] of the optical system should be as high as possible.

To quantify how etendue and other filter metrics limit tissue imaging depth, consider that the goal is to reach a signal to noise ratio (SNR) that is good enough to reliably identify an embedded object. From Rose's criteria,[13] this is possible if the SNR > 5. Assuming sufficiently advanced classical noise suppression techniques are used, the SNR will eventually be limited by quantum statistics or shot noise. Considering only tagged light shot noise, the required SNR can be achieved by collecting at least 25 photons per image pixel, assuming a high contrast embedded object. If background light is present then its shot noise must also be considered. Assuming a signal to background ratio (SBR) that is independent of laser illumination intensity, the result is that a factor of 1/SBR more tagged (signal) photons are required to overcome background noise, assuming SBR $\ll 1$. Thus to get sufficient SNR for weak signals, the optical filter must strongly suppress untagged light to increase the SBR, yet it must not attenuate the tagged light and therefore should have as high etendue as possible.

In Figure 1(b), the etendue of the leading UOT filtering techniques is compared to that of biological tissue. As seen, the lowest etendue filter is the confocal Fabry-Perot (FP) filter,[14] even though this technology has demonstrated the deepest tissue imaging until now. To achieve this, a very high laser power was used to give more tagged photons. The next higher etendue is the photorefractive (PR) filter.[15] This technology is based on real time holography which is like a high-etendue version of heterodyne detection. By far, the highest reported etendue is a Tm:YAG spectral hole burning (SHB) filter[16] since the SHB crystal itself has a maximal 90° acceptance half-angle.

Here, we make use of a persistent spectral hole burning (PSHB) optical filter which is a special class of SHB materials that have a long hole lifetime, seconds or longer. This long lifetime allows the use of complex hole burning pulse sequences that can give unprecedented performance as a spectral filter; for example using a carefully selected spatial geometry, 140 dB discrimination has been demonstrated in praseodymium doped yttrium silicate (Pr:YSO),[17] for collimated laser light, with better than 50% transmission in the passband.

The basic experimental setup for deep tissue UOT with PSHB filtering is shown in Figure 2(a). Diffuse light from the object of interest is collected by a high numerical aperture (NA) lens and funneled into the front face of the hole burning crystal. Once inside the crystal, the light is guided to the exit face via total internal reflection. Since this waveguiding is independent of crystal length, very long crystals can be used to achieve a high optical absorption of untagged light. The filtered tagged light exiting the crystal is then collected by another high NA lens and imaged onto a sensitive optical detector, for example a photon counter.

To demonstrate deep tissue imaging with slow light enhanced spectral hole filtering, experiments were performed on tissue-mimicking phantoms and real tissue (chicken breast), as illustrated in Figure 3. Here, Figure 3(a) shows a typical 1D image in the ultrasound propagation direction (A-line) for two absorbing objects buried inside a 4.5 cm thick (in the laser propagation direction) tissue phantom, having a reduced scattering coefficient of 10 cm^{-1}. As seen a high contrast image of the absorbing objects is produced, but there is significant untagged background light.

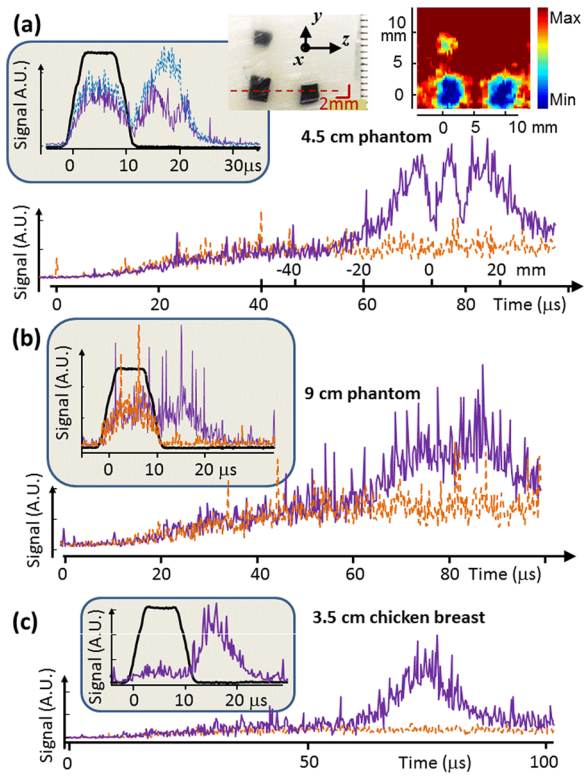

FIG. 3. (a) Images of buried (optically absorbing) objects in a 4.5 cm thick (x-direction) tissue phantom. The plotted data show a 1-D A-line image, and a 2-D image (B-mode tomogram) is shown above, along with a cutaway photo of the embedded objects. The smaller 2 mm object in the B-mode shows reduced contrast and hence this is the resolution limit. The upper (solid) A-line data is with ultrasound present and the lower (dashed) plot without. Both images are 50 trace accumulations, and the B-mode is interpolated and median filtered. The inset shows A-line imaging with slow light. The delayed light shows a high contrast dip when 3.5 mm thick absorbing object is present (solid). The data without an absorber (dashed) is superimposed, for comparison. (b) Ultrasound tagged light (A-traces) from a 9 cm thick tissue-mimicking phantom with ultrasound applied(upper solid line) and without (lower dashed line). These A-lines are 500 accumulations. The inset shows additional slow light filtering. Here, a significant delayed component is seen with ultrasound present (solid line) but only detector dark noise is seen at the same delay time without ultrasound (dashed line). The dark line shows the input laser pulse. (c) Ultrasound tagged light detected in 3.5 cm thick chicken breast tissue, with ultrasound (upper solid line) and without (lower dashed line). The inset shows additional filtering with slow light. The dark line shows the reference optical pulse. These A-lines were averaged 500 times.

TABLE I. Projections for ultimate imaging depth in tissue phantoms assuming real-time video rate imaging. Here video rate is defined as a frame rate of 35 frames/s for a 2D image with 30 lines.

Parameter		Present setup	Best possible	Unit	Improvement factor
Laser energy	Power	0.1	240	W	2400
	Duration	10	10	μs	1
Ultrasound	Pressure	4	4	Mpa	1
	Duration	2	2	cycle	1
Filter etendue		3	900	sr-mm^2	300
Passband transmission		0.3	0.3		1
Detector quantum efficiency		0.07	0.8		10
Tagged photo-counts/0.5 μs_pixel/shot		0.04	290 K	Photo-counts	7 M
dB above (25 counts/pixel)		−28	+40	dB	+68 dB
Single shot depth (4.4 dB/cm)		3	18	cm	+15 cm

To remove this background, slow light was used to selectively delay the tagged light, as shown by the A-line images in the inset of Figure 3(a). Slow light naturally arises from the steep refractive index dispersion in the passband of a deep spectral hole (see Figure 2(d)).[4,18] Conversely, since the dispersion is relatively flat in the absorbing region several hole widths away, any untagged light leaking through the crystal is not significantly slowed. For an optical pulse whose spectral width is matched to that of the spectral hole passband, the delay measured in pulse widths will be proportional to the optical density in the surrounding absorbing region.[4] The quality of the data that can be obtained strongly depends on the filter characteristics (transmission, suppression, steepness, etc.) and extensive work has been investigated in optical pumping techniques important for the filter creation.[19] For our 2.3 MHz ultrasound frequency, a 2 cycle pulse is about 1 μs long, and a light pulse of this length is easily delayed many pulse widths as seen in Figure 2(e). In the inset of Figure 3(a)), a much longer probe pulse was used so as to image an entire buried object in one A-line, but a full pulse-width delay can still be achieved.

Figure 3(b) illustrates the limits of persistent spectral filtering with and without slow light, using a much thicker 9 cm tissue phantom. Again both long and short optical illumination pulses are used to illustrate the advantage of slow light delay. As seen in the inset of Figure 3(b), the delayed ultrasound tagged light is well separated from the untagged light background, and furthermore, data taken without ultrasound present show no visible untagged light at the relevant delay times (i.e., it is indistinguishable from detector dark noise). From this data, we estimate a lower limit of 16 for the signal to background ratio. Such a large SBR is unprecedented for so thick a phantom and clearly shows the multiplicative filtering capability of slow light, as the untagged background has already been suppressed 30 dB by the spectral hole filter in the long pulse illumination case.

Figure 3(c) (inset) shows that slow light also effectively separates tagged light from the untagged background in real tissue (chicken breast). Here, a much thinner sample, 3.5 cm thick, was needed as the 606 nm illumination was more strongly absorbed than in the phantom.

It is of interest to estimate the thickest tissue sample that can be imaged in real time (video rate) using slow light enhanced spectral hole burning filters. In the current setup, there are too few signal photons to acquire real time images from the 9 cm thick phantom since the tagged light amounts to only about 4 photon counts per 100 ns data bin with a 500 trace accumulation. However, by increasing the laser illumination intensity to 1/10 of the 2.4 kW laser safety limit,[20] increasing the etendue up to the limit imposed by the cryostat for the present crystal diameter, and using a higher quantum efficiency photon counter, we project ~290 k photo-counts per image pixel for a single shot A-line with a pixel width of 500 ns (1 cycle of ultrasound). Since only 25 counts are needed to satisfy Rose's criteria for a high contrast object, there would be 14 000 times more photo-counts than needed for video rate imaging at this 9 cm depth. These extra photons could be used to see even deeper into tissue, as illustrated in Table I. In this table, the surplus photo-counts are converted into additional tissue thickness using the measured 4.4 dB/cm signal attenuation to arrive at the 18 cm thickness projection for single-shot A-lines in phantoms.

Note that the projections in Table I neglect the effects of background which would reduce the ultimate imaging depth. From Figure 3(b), it is seen that the SBR ~ 1 for the 9 cm tissue phantom using spectral hole filtering alone. Since the PSHB spectral filtering discrimination is already degraded to 30 dB for diffuse light, it is expected that the extra SBR enhancement provided by slow light will be essential for achieving the goal deep tissue imaging at video rates.

Clearly, video rate imaging at such tissue depths is approaching that needed for clinical applications if it can be extended to real tissue. The validity of using tissue phantoms to model imaging performance in real tissue was recently demonstrated at 1.06 μm, where both real tissue and phantoms of the same thickness showed similar image quality.[14] While no candidate PSHB materials exist at 1.06 μm, Tm:YAG operating at 793 nm is still within the therapeutic window has shown to be capable of persistent spectral holes with up to 30 s lifetimes[21] and could eventually realize the elusive goal of deep tissue imaging for certain clinical applications.

S.K. was sponsored in part by the Swedish Research Council, the Knut & Alice Wallenberg Foundation, the Crafoord Foundation and the EC FP7 Contract No. 247743 (QuRep). L.V.W. was sponsored in part by National Institutes of Health grants R01 EB000712 and U54 CA136398.

[1]C. Kim, K. H. Song, and L. V. Wang, J. Biomed. Opt. **13**(2), 020507 (2008).
[2]L. V. Wang and Hsin-i Wu, *Biomedical Optics: Principles And Imaging* (Wiley, Hoboken, NJ, 2007).
[3]L. V. Hau, S. E. Harris, Z. Dutton, and C. H. Behroozi, Nature **397**(6720), 594 (1999); F. Morichetti, C. Ferrari, A. Canciamilla, and A. Melloni, Laser Photonics Rev. **6**(1), 74 (2012); K. F. Reim, P. Michelberger, K. C. Lee, J. Nunn, N. K. Langford, and I. A. Walmsley, Phys. Rev. Lett. **107**(5), 053603 (2011); M. Salit and M. S. Shahriar, J. Opt. **12**(10), 11 (2010).
[4]R. N. Shakhmuratov, A. Rebane, P. Mégret, and J. Odeurs, Phys. Rev. A **71**(5), 053811 (2005).
[5]L. V. Wang, *Photoacoustic Imaging and Spectroscopy* (CRC, Boca Raton, 2009).
[6]R. J. Dewhurst and Q. Shan, Meas. Sci. Technol. **10**(11), R139 (1999).
[7]C. E. Brown and M. F. Fingas, Mar. Pollution Bull. **47**(9-12), 485 (2003).
[8]X. Xu, H. Zhang, P. Hemmer, De-kui Qing, C. Kim, and L. V. Wang, Opt. Lett. **32**(6), 656 (2007).
[9]M. W. Sigrist, *Air Monitoring by Spectroscopic Techniques* (Wiley, New York, 1994).
[10]L. V. Wang, Nat. Photonics **3**(9), 503 (2009).
[11]M. Kempe, M. Larionov, D. Zaslavsky, and A. Z. Genack, J. Opt. Soc. Am. A **14**(5), 1151 (1997).
[12]R. Winston, W. T. Welford, J. C. Miñano, and P. Benítez, *Nonimaging Optics* (Academic, Boston, MA, 2005).
[13]J. T. Bushberg, *The Essential Physics of Medical Imaging*, 2nd ed. (Lippincott Williams & Wilkins, Philadelphia, 2002).
[14]G. Rousseau, A. Blouin, and J.-P. Monchalin, Opt. Lett. **34**(21), 3445 (2009).
[15]F. Ramaz, B. Forget, M. Atlan, A. C. Boccara, M. Gross, P. Delaye, and G. Roosen, Opt. Express **12**(22), 5469 (2004).
[16]Y. Li, H. Zhang, C. Kim, K. H. Wagner, P. Hemmer, and L. V. Wang, Appl. Phys. Lett. **93**(1), 011111 (2008); Y. Li, P. Hemmer, C. Kim, H. Zhang, and L. V. Wang, Opt. Express **16** (19), 14862 (2008).
[17]M. P. Hedges, J. J. Longdell, Y. Li, and M. J. Sellars, Nature **465**(7301), 1052 (2010).
[18]A. Walther, A. Amari, S. Kröll, and A. Kalachev, Phys. Rev. A **80**(1), 012317 (2009).
[19]M. Nilsson, L. Rippe, S. Kröll, R. Klieber, and D. Suter, Phys. Rev. B **70**(21), 214116 (2004); L. Rippe, M. Nilsson, S. Kröll, R. Klieber, and D. Suter, Phys. Rev. A **71**(6), 062328 (2005); M. Nilsson, L. Rippe, N. Ohlsson, T. Christiansson, and S. Kröll, Phys. Scr. **2002**(T102), 178 (2002); A. Amari, A. Walther, M. Sabooni, M. Huang, S. Kröll, M. Afzelius, I. Usmani, B. Lauritzen, N. Sangouard, H. de Riedmatten *et al.*, J. Lumin. **130**(9), 1579 (2010).
[20]American National Standard for the Safe Use of Lasers, Standard Z136.1-2000 (ANSI, Inc., New York, 2000).
[21]N. Ohlsson, M. Nilsson, S. Kröll, and R. Krishna Mohan, Opt. Lett. **28**(6), 450 (2003).